CALIFORNIA STATE UNIVERSITY, NORTHRIDGE

Many-Body Localization and Mobility Edge in Spin Chain Systems With Quasiperiodic Fields

A thesis submitted in partial fulfillment of the requirements

For the degree of Master of Science in Physics

By

Thomas R. Look

May 2018

The thesis of Thomas R. Look is approved:

Dr. Say-Peng Lim	Date
Dr. Yohannes Shiferaw	Date
Dr. Donna Sheng, Chair	Date

California State University, Northridge

Acknowledgements

This thesis is the result of an unexpected journey and would not be possible without the tremendous support I have received over the past few years. I was quite naive when I came to CSUN as a physics neophyte, knowing only that I wanted to learn about physics and wanting to challenge myself and test the bounds of my abilities. I am lucky to have encountered so many who have encouraged and inspired me. I would like to thank—in particular—Donna Sheng, Say-Peng Lim, and Yohannes Shiferaw for their constant support and guidance. I would also like to thank Mac Lee with whom I've spent countless hours discussing everything from physics to politics, and whose friendship and rivalry has helped keep me motivated. I would also like to thank the Association of Retired Faculty and the Graduate Fellowship for Outstanding Research Promise in Science and Mathematics from the College of Science and Mathematics here at CSUN which helped to fund this research.

Table of Contents

List of Figures

List of Tables

Abstract

Many-Body Localization and Mobility Edge in Spin Chain Systems With Quasiperiodic Fields

By

Thomas R. Look

Master of Science in Physics

The study of many-body localization (MBL) helps address questions at the very foundation of quantum statistical mechanics—chiefly, can an isolated quantum system serve as a thermal bath for its own subsystems? We study the many-body localization of spin chain systems with quasiperiodic fields. Based on finite-size scaling analysis of entanglement entropy and fluctuations of the bipartite magnetization, we identify $W_c > 1.85$ as a lower bound for the critical disorder necessary to drive the MBL phase transition. We also examine the entanglement entropy of an initial product state after a global quantum quench where we find power-law and logarithmic growth for the thermal and many-body localized phases, respectively, with a transition point $W_c \sim 2.5$. For larger disorder strength, both imbalance and spin-glass order are preserved at long times, while spin-glass order shows dependence on system size. We also observe the appearance of a mobility edge in small quasiperiodic systems and explore density matrix renormalization group methods to probe larger systems. Quasiperiodic fields have been applied in different experimental systems, and our study finds that such fields are very efficient at driving the many-body localized phase transition.

Chapter 1

Introduction to many-body localization

In the presence of strong enough disorder, an isolated interacting many-body system can fail to quantum thermalize on any timescale. This phenomenon, known as many-body localization (MBL), is a distinct phase of matter that challenges fundamental assumptions at the very foundation of quantum statistical mechanics. The study of MBL is important, both for the theoretical foundation of quantum statistical mechanics and for valuable insights that might be gained for building future quantum devices.

1.1 Localization in non-interacting systems

In 1958, while band theory was seeing overwhelming success, P.W. Anderson published his seminal paper, *Absence of Diffusion in Certain Random Latices* [1]. Emphasizing locality, in opposition to prevailing wisdom, Anderson sought "...to lay the foundation for a quantum-mechanical theory of transport..." [1]. While this effort did not receive much immediate attention, he was later awarded the 1977 Nobel Prize in Physics in part for this work. The essence of his theory was that randomness in the distribution of impurities or defects in a lattice could permanently pin down an eigenstate of non-interacting electrons to a given region preventing the conduction of charge and heat. This effect is now known as Anderson Localization.

We can understand this effect by studying a tight binding model with Hamiltonian,

$$H = \sum_{i \neq j} (V_{ij} c_i^\dagger c_j + h.c.) + \sum_i E_i c_i^\dagger c_i, \tag{1.1}$$

where $c_i^\dagger$ is the fermionic creation operator for site i, on-site energy E_i is a stochastic variable with probability distribution $P(E)dE$ characterized by width W, and V_{ij} is the

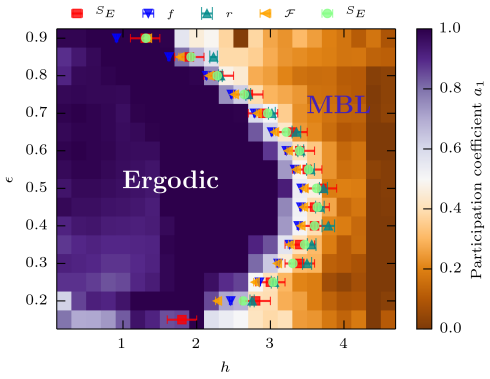

Figure 1.1: Phase diagram for MBL in random field models obtained from ED studies. At strong enough disorder h, both ergodic and MBL phases appear in the energy spectrum. From Ref. [23]

.

hopping matrix element between site i and site j. In one dimension, the eigenstates of this Hamiltonian are exponentially localized, which Anderson was able to demonstrate with a perturbative analysis.

1.2 Localization in interacting systems

Anderson's theory was a simplification of the systems in Feher's experiments since it ignored electron-electron interactions. The work of Basko, Aleiner, and Altshuler [2] in 2006, extended localization into the weakly interacting regime and proved, to all orders of perturbation theory, the existence of a finite temperature metal-insulator transition in these systems. Driving the metal-insulator transition was the appearance of a many-body mobility edge between localized and thermal (ergodic) eigenstates in the energy spectrum. This work helped spark a flurry of research activity that continues today [3–55, 55–72]. A spin chain model was introduced by Pal and Huse [4] providing a method of studying MBL systems through exact diagonalization (ED). While early ED studies showed evidence of a many-body mobility edge [23, 29, 51, 73], the actual picture is not clear as we will discuss in Chapter 3.

1.3 Entanglement Entropy

Quantum entanglement has been a most curious feature of quantum theory ever since it was first conceptually introduced by Einstein, Podolsky, and Rosen in an attempt to curtail the ascendancy of quantum mechanics [74]. A bipartite system, with subsystems A and B, is said to be quantum entangled when the state of A cannot be described independently of B. Let $\mathcal{H}_{AB}$ be the Hilbert space for a composite system of A and B, then $\mathcal{H}_{AB} = \mathcal{H}_A \otimes \mathcal{H}_B$, with $\mathcal{H}_A$ and $\mathcal{H}_B$ of dimension N_A and N_B respectively. The state $|\psi\rangle \in \mathcal{H}_A \otimes \mathcal{H}_B$ can be written as

$$|\psi\rangle = \sum_{i,j} c_{ij} \, |\alpha_i\rangle_A \, |\beta_j\rangle_B \,, \tag{1.2}$$

where c_{ij} are elements of rectangular matrix C of dimension $(N_A \times N_B)$ and $\{|\alpha_i\rangle_A\}$ and $\{|\beta_j\rangle_B\}$ are orthonormal bases of A and B respectively. The density matrix for the state is given by

$$\rho = |\psi\rangle \, \langle\psi| \,. \tag{1.3}$$

The reduced density matrix for subsystem A is obtained by taking the partial trace over subsystem B

$$\rho_A \equiv \sum_{j}^{N_B} \, {}_B\langle\beta_j|\rho|\beta_j\rangle_B = \mathrm{Tr}_B(\rho). \tag{1.4}$$

Similarly, a partial trace over A yields the reduced density matrix ρ_B

$$\rho_B \equiv \sum_{i}^{N_A} \, {}_A\langle\alpha_i|\rho|\alpha_i\rangle_A = \mathrm{Tr}_A(\rho). \tag{1.5}$$

It can also be shown that the reduced density matrices can be constructed from the coefficient matrix C as follows:

$$\rho_A = CC^\dagger \qquad \rho_B = C^\dagger C. \tag{1.6}$$

The *entanglement entropy* S_{AB} is defined as the von Neumann entropy of the reduced density matrix ρ_A:

$$S_{AB} \equiv -\mathrm{Tr}(\rho_A \ln \rho_A) = -\sum_{a=1}^{N_A} w_a \ln w_a, \tag{1.7}$$

where w_a are the eigenvalues of the reduced density matrix ρ_A. As we will soon prove, the entanglement entropy is the same regardless of whether ρ_A or ρ_B is used.

For any rectangular matrix M of dimension $(N_A \times N_B)$, with $N \equiv \min(N_A, N_B)$, there exists a *singular value decomposition* (SVD) such that

$$M = USV^\dagger, \tag{1.8}$$

where U has dimensions $(N_A \times N)$ with orthonormal columns, $V^\dagger$ has dimensions $(N \times N_B)$ with orthonormal rows, and S is a semidefinite diagonal matrix of dimension $(N \times N)$ with elements $S_{aa} \equiv s_a$ known as *singular values*. The $r \leq N$ nonzero singular values are given in descending order such that $s_1 \geq s_2 \geq \cdots \geq s_r > 0$.

The SVD of the coefficient matrix C gives

$$C_{ij} = \sum_{a=1}^{N} U_{ia} S_{aa} V^*_{ja}. \tag{1.9}$$

By inserting Eq. (1.9) into Eq. (1.2), we find

$$\begin{aligned} |\psi\rangle &= \sum_{i,j} \sum_{a=1}^{N} U_{ia} S_{aa} V^*_{ja} |\alpha_i\rangle_A |\beta_j\rangle_B \\ &= \sum_{a=1}^{N} \left(\sum_i U_{ia} |\alpha_i\rangle_A \right) s_a \left(\sum_j V^*_{ja} |\beta_j\rangle \right) \\ &= \sum_{a=1}^{N} s_a |a\rangle_A |a\rangle_B , \end{aligned} \tag{1.10}$$

Thermal phase	Single-particle localized	Many-body localized
Memory of initial conditions 'hidden' in global operators at long times	Some memory of local initial conditions preserved in local observables at long times	Some memory of local initial conditions preserved in local observables at long times.
ETH true	ETH false	ETH false
May have non-zero DC conductivity	Zero DC conductivity	Zero DC conductivity
Continuous local spectrum	Discrete local spectrum	Discrete local spectrum
Eigenstates with volume-law entanglement	Eigenstates with area-law entanglement	Eigenstates with area-law entanglement
Power-law spreading of entanglement from non-entangled initial condition	No spreading of entanglement	Logarithmic spreading of entanglement from non-entangled initial condition
Dephasing and dissipation	No dephasing, no dissipation	Dephasing but no dissipation

Table 1.1: A list of some properties of the many-body-localized phase, contrasted with properties of the thermal and the single-particle-localized phases. Taken from Ref. [7]

where $\{|a\rangle_A\}$ and $\{|a\rangle_B\}$ are new orthonormal bases sets for A and B, and $\sum_a s_a^2 = 1$. Truncating this sum for $r \leq N$ nonzero singular values gives the *Schmidt decomposition*

$$|\psi\rangle = \sum_{a=1}^{r} s_a |a\rangle_A |a\rangle_B . \tag{1.11}$$

If we use Eq. (1.11) in Eq. (1.4) and Eq. (1.5) we find that the reduced density matrices can be written as

$$\rho_A = \sum_{a=1}^{r} s_a^2 |a\rangle_A \ {}_A\langle a| \qquad \rho_B = \sum_{a=1}^{r} s_a^2 |a\rangle_B \ {}_B\langle a| \tag{1.12}$$

It is then obvious that $w_a = s_a^2$ and that the von Neumann entropy for ρ_A and ρ_B are the same. The von Neumann entropy can then be written as

$$S_{AB} = -\sum_{a=1}^{r} s_a^2 \ln s_a^2. \tag{1.13}$$

From here we can see the two extremes for entanglement entropy. If $r = 1$, then $s_1 = 1$, and Eq. (1.11) reduces to a pure product state $|\psi\rangle = |a\rangle_A |a\rangle_B$ with entanglement entropy $S_{AB} = 0$. A maximally entangled state is achieved when $r = N$ and $s_a^2 = 1/N$, giving entanglement entropy $S_{AB} = \ln N$. For an equally partitioned chain of L spins, $N = 2^{L/2}$, thus $S_{AB} = (L/2)\ln 2$ gives the volume-law bound for the chain.

The entanglement entropy has emerged as an important quantity in the study of MBL and thermal systems [4, 17, 23, 28, 29, 51]. As seen in Table 1.1 taken from Ref. [7], the entanglement entropy of MBL systems is bound by the area-law—maximal entanglement entropy proportional to the surface area of the boundary between subsystems—and experiences logarithmic spreading of entanglement up to this bound. Meanwhile, the thermal phase is bound by the volume-law—entanglement entropy proportional to the volume of the system—and experiences power-law spreading of entanglement.

Chapter 2

Many-body localization in spin chain systems with quasiperiodic fields

The existence of both the ergodic and MBL phases dictates a novel dynamic quantum phase transition between them [2–4, 17, 21, 22, 29, 49–54, 56, 75]. Random disorder introduces rare Griffiths regions [22, 49, 50, 54, 59, 60, 75] which may have singular contributions in driving such a phase transition, but there is still a limited quantitative understanding of their effects. Quasiperiodic fields [76] have a period incommensurate with the lattice constant, thus they break translational invariance and introduce disorder in a more controlled way when compared to random fields.

In a recent work, it was shown that interacting quasiperiodic models can have an MBL phase [31], and signatures of this phase have been experimentally observed in recent cold-atom experiments [61–64, 77]. However, most numerical studies of the MBL transition have focused on models of spin chains with random fields [4, 22, 23, 54, 75]. Very recently, the dynamic quantum phase transition has been analyzed [38, 55, 65, 67] for systems with quasiperiodic potentials. By analyzing the intra-sample and inter-sample fluctuations with a close comparison between quasiperiodic and random fields, Khemani, et al. [55], have demonstrated the possibility of two universality classes for the quantum phase transition [55, 75]. Other studies explore the interplay of MBL in quasiperiodic potentials and the single-particle mobility edge [65, 68, 69]. Time evolution of many-body systems have been studied for spin-chains with randomly distributed fields [29, 70] and quasiperiodic fields [67], which can be used to address the dynamics of the thermal to MBL phase transition [7, 49, 50]. After a global quantum quench, the power-law growth of bipartite entanglement entropy is observed for thermal states while logarithmic growth is found for MBL states where local memories of an initial product state persist for all time [38, 70].

In this chapter we report on eigenstate and time-dependent studies of spin chains with quasiperiodic fields. Through exact diagonalization (ED) and Lanczos Krylov space time

evolution calculations, we find a dynamic quantum phase transition from the ergodic phase to the MBL phase that is similar to spin chains with random disordered fields. However, systems with quasiperiodic fields appear to be more efficient at localizing quantum states which is demonstrated by a smaller critical disorder, $W_c \sim 1.85$ (as a lower bound) compared to similar estimate for systems with random fields [23] (where the critical disorder field strength is around 3.5 [23]) in agreement with the work of Khemani, et al. [75] We also evolve a randomly selected initial product state and study how entanglement entropy and other observables behave as a function of time. Similar to random field systems, we find that bipartite entanglement entropy experiences power-law growth in the thermal phase and logarithmic growth in the MBL phase. Interestingly, we also observe quasiperiodic oscillations of spin imbalance on short timescales. Preservation of imbalance and spin glass order at long times is characteristic of the MBL phase, commensurate with stronger disorder. Our results suggest a critical quasiperiodic field strength of $W_c \sim 2.5$, and provide a quantitative understanding of the MBL phase for spin systems with quasiperiodic fields.

2.1 Theoretical model and ergodic to many-body localized phase transition

We study the Heisenberg spin-1/2 chain with a quasi-periodic field

$$H = J \sum_{i=1}^{L-1} \mathbf{S}_i \cdot \mathbf{S}_{i+1} + W \sum_{i}^{L} \cos(2\pi c i + \phi) S_i^z. \tag{2.1}$$

where $\mathbf{S}_i$ is the spin operator for site i, J is the nearest neighbor coupling constant which we set to $J = 1$, W is the strength of the quasi-periodic field, c is an irrational wave number chosen to be $c = \sqrt{2}$, and ϕ is a random phase used to create different quasiperiodic field configurations. L is the number of sites (system length). This model is similar to the one studied recently in [55], which included second nearest neighboring transverse spin couplings. In this work, however, we focus on the time-evolution of initial product states

for systems with quasiperiodic fields. We use open-boundary condition which allows for a larger window to observe the time evolution of physical quantities [70] before they saturate due to finite-size effects.

We perform ED calculations to obtain energy eigenstates around the energy E at a target energy density ε [23] for systems with different number of sites $L = 10 - 18$ in the total $S_z = 0$ sector. Specifically, for each quasiperiodic field configuration, we first calculate the ground state energy E_0 and the maximum energy $E_{\max}$, which are used to define the target energy density $\varepsilon = (E - E_0)/(E_{\max} - E_0)$. We first locate the critical point for the MBL phase transition based on the entanglement entropy and the fluctuations of the half-system magnetization [23]. The Von Neumann entanglement entropy of a system partitioned in the middle, with reduced density matrix ρ_A, is given by $S = -\mathrm{Tr}(\rho_A \ln \rho_A)$. We average the bipartite entanglement entropy over 30 ($L = 10$) to 200 ($L = 18$) eigenstates near target energy E characterized by energy density $\varepsilon = 0.5$, and over 1000 quasifield configurations by choosing random ϕ between $(0, 2\pi)$. As shown in Fig. 2.1(a), we plot the ratio of entanglement entropy over the number of system sites S/L for different systems at energy density $\varepsilon = 0.5$ from $L = 10$ to 18 as a function of quasiperiodic field strength W. As $W \to 0$ we see S/L increases with L which approaches the Page value ($S/L \sim 0.5 \ln(2)$ for large L limit) [78] following the volume law of the ergodic phase. For larger W, S/L approaches zero indicating area law entanglement and non-ergodic behavior where the MBL state is realized. With varying W, all data points approximately cross each other around a critical value $W_c \sim 1.85$. We compare the entanglement entropy behavior with the bipartite fluctuations F of the subsystem magnetization S_A^z [23, 72], which is defined as $F = \langle {S_A^z}^2 \rangle - \langle S_A^z \rangle^2$ as shown in Fig. 2.1(b). We see that F/L increases on the small W side, while it becomes vanishingly small on the larger W side. The F/L curves for different L approximately cross each other around the critical field strength $W_c \sim 1.85$, consistent with the behavior of the entanglement entropy. In fact, we see that there is an approximately proportional relationship between S and F for all W region. We also note that the crossing

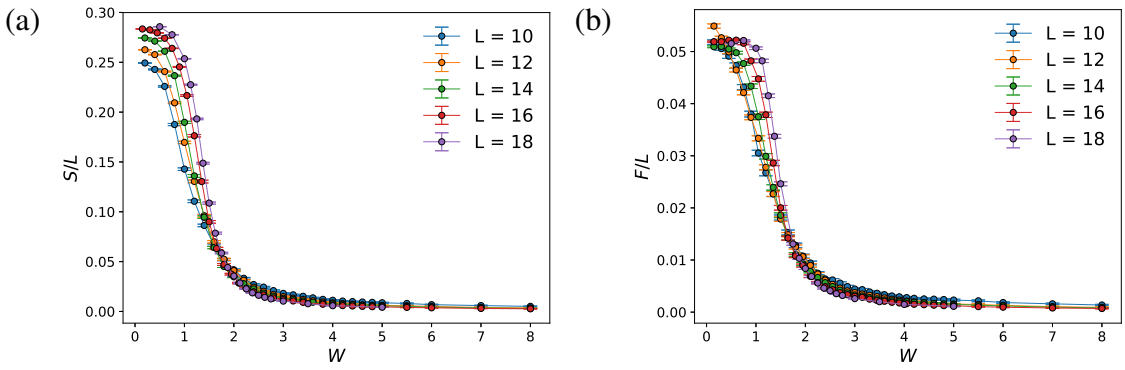

Figure 2.1: (a) The ratio of entanglement entropy over the number of system sites S/L for $L = 10 - 18$ at the energy density $\varepsilon = 0.5$ as a function of the strength of the quasiperiodic fields W. (b) The fluctuations of the half system magnetization over L for $L = 10 - 18$. Both graphs display crossing around $W_c \sim 1.85$, suggesting a quantum phase transition at that point. For larger system sizes, the crossing point drifts towards larger W.

points between larger L curves move towards the larger W side. This feature was also observed in a different model for quasiperiodic systems as well as for random disorder systems [55, 75], which indicates the W_c we observed is a lower bound for the critical point of the dynamic quantum phase transition.

We now analyze the finite-size scaling properties of the MBL transition for the quasiperiodic field model. Crossing the quantum phase transition, we expect that the entanglement entropy ratio S/S_T and the fluctuations of the half system magnetization over the system length F/L should be a function of $L/\xi \sim L(W - W_c)^\nu$, where the correlation length ξ has power-law divergence at the transition point with an exponent ν. Note that $S_T = 0.5(L \ln(2) - 1)$ is the saturated thermal value for the entanglement entropy of a finite size system [55, 78]. As shown in Fig. 2.2(a-b), we find that these quantities for all system lengths can indeed be collapsed into one curve in a form $f((W - W_c)L^{1/\nu})$ by using the proper critical $W_c \sim 1.85 - 1.95$ and the scaling exponent $\nu \sim 1.1 \pm 0.1$, which give the best collapsing effect. The obtained exponent ν is in agreement with the results of Khemani et al. [55], although the fitting for the F/L shows much larger finite-size effect. Similar crossing point is also obtained using the adjacent gap ratio [23] (with slightly larger finite-size effect),

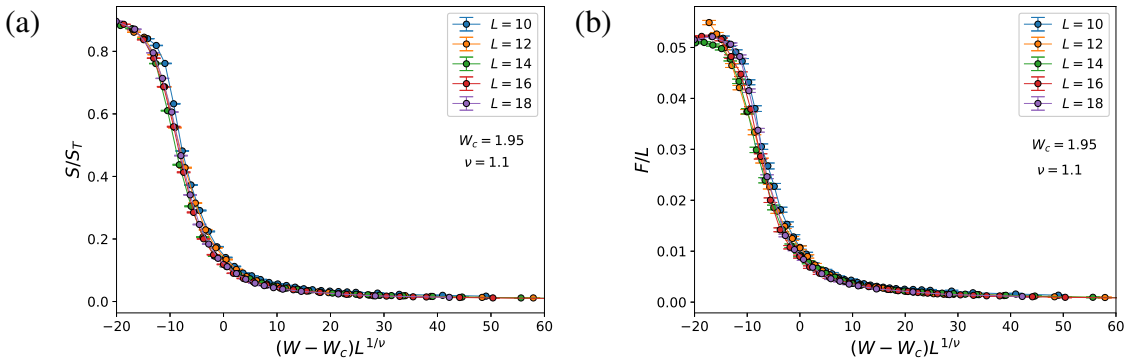

Figure 2.2: (a) Finite-size scaling collapse for (a) entanglement entropy S/S_T with S_T as the Page value [78] , and (b) the fluctuations of the half-system magnetization data in the quasiperiodic model for the system sizes $L = 10 - 18$. The critical disorder strength $W_c \sim 1.85 - 1.95$ and scaling exponent $\nu \sim 1.1$ are used to best collapse the data.

indicating a transition between the Gaussian orthogonal ensemble statistics and Poisson statistics consistent with the thermal and MBL phases, respectively.

2.2 Time-evolution of quantum states

We study the non-equilibrium quantum dynamics of the quasiperiodic systems after a global quantum quench. Here we start by selecting a product state $|\Psi(0)\rangle = |\sigma_1, \sigma_2, \ldots, \sigma_L\rangle$ with an average energy close to the target energy determined by the energy density $\varepsilon = 0.5$ at the time $t = 0$ after the quench, where $\sigma_i = \pm$ represents the spin-z component $\pm 1/2$ (with $\hbar = 1$) at site i. The state at time t can be obtained as $|\Psi(t)\rangle = e^{-iHt}\,|\psi(0)\rangle = e^{-iH\Delta t}\,|\psi(t - \Delta t)\rangle$. We calculate the time evolution of an initial state $|\Psi_0\rangle$ based on a projection of the Hamiltonian to the Krylov space spanned by $|\Psi_0\rangle$, $H\,|\Psi_0\rangle$, $\ldots$, $H^n\,|\Psi_0\rangle$. We calculate all eigenstates in this space to obtain the time-evolution operator [23]. Using a reasonably small time step $\delta t \sim 0.2/J$ allows for highly accurate results for the quantum state with a small $n = 30 - 60$. All time-evolution results are being averaged over more than 500 quasiperiodic field configurations.

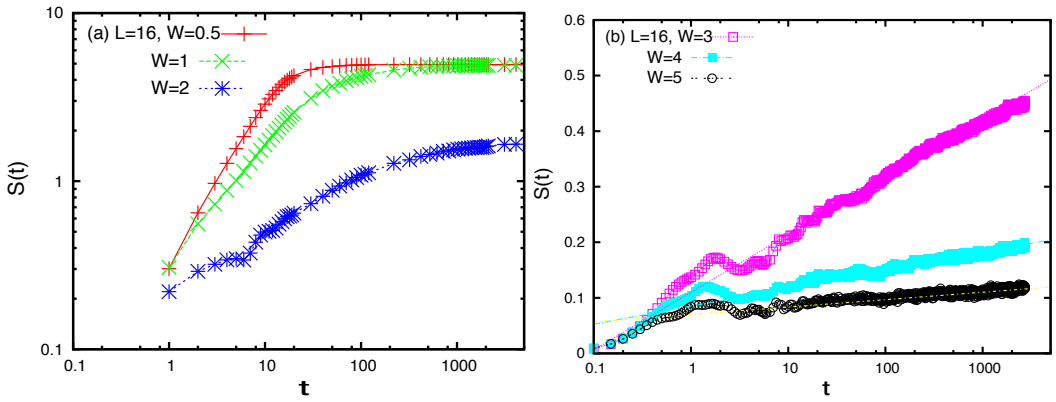

Figure 2.3: (a) In this log-log plot, for systems with $W < W_c$ we observe power-law growth of entropy $S(t)$ which saturates at the $L = 16$ Page value. (b) Semi-log plot of $S(t)$ with $W > W_c$ indicating logarithmic growth of $S(t)$. The error bars of data are at the same order as the size of symbols.

We first discuss the general behavior of the entanglement entropy as a function of time. On the small W side shown in Fig. 2.3(a), we find that the entropy $S(t)$ exhibits power-law growth in time t before it reaches the saturated value $\frac{L}{2}\ln 2$ at long time limit in agreement with the ETH. On the larger W side, we find a much slower growth, which can be fit with a logarithmic growth function as shown in Fig. 2.3(b) for $W = 3-5$. We now analyze the finite-size scaling behavior of $S(t)$ for $L = 12-20$. For small $W = 1$ as shown in Fig. 2.4(a), we find that the initial growth ($t \sim 1$) of $S(t)$ is very rapid and system size independent. For the intermediate time regime, $S(t)$ experiences power-law growth as demonstrated by the linear behavior in the logarithmic plots until the finite-size effect sets in. With the increase of L, we find a wider time interval for the power-law growth of $S(t)$. Interestingly, we see very similar behavior and a smaller window for power-law growth of $S(t)$ for $W = 2$. The power-law growth indicated by the straight line in the Fig. 2.4(b) is clearest for larger system size $L = 20$. This is a strong indication that the $W = 2$ is in the thermal phase consistent with the moving of the crossing point toward larger W with the increase of L observed in Fig. 2.1. We then look into $S(t)$ at $W = 3$ as shown in Fig. 2.4(c) where we observe that for small t, $S(t)$ grows rapidly while the initial product state evolves to a superposition state for $t \sim 1$, which is then followed by some oscillations of $S(t)$. With further increase of t,

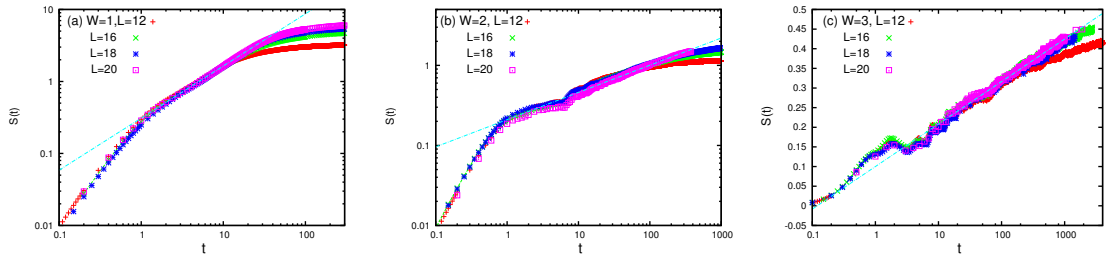

Figure 2.4: (a) For system sizes ranging from 12 to 20, at $W = 1$, we observe that $S(t)$increases rapidly until $t \sim 1$. When $1 < t < 50$, $S(t)$ for all L data fit into a straight line demonstrating robust power-law growth. For larger t, we see that $S(t)$ saturates toward $\frac{L}{2} \ln 2$, consistent with the thermal entropy of the ergodic phase. (b) At $W = 2$, for smaller system sizes, we observe that $S(t)$ grows slower than predicted by the power-law; on the other hand, $L = 20$ results behave as expected for a thermal state and the growth of its entropy over time follows the power-law. (c) At $W = 3$, we notice that all $S(t)$ plots fit to a straight line in the semi-log plot, indicating logarithmic growth for the MBL state.

we find a logarithmic growth of $S(t)$ for a time range of more than two orders of magnitude. The range of t for logarithmic growth of $S(t)$ becomes larger with the increase of W. These results confirm an MBL phase with similar behavior to the random field case studied by Luitz, et al [23].

Now we turn to spin correlations during the time evolution. We start from the product state $|\Psi(0)\rangle$ where the S_i^z on each site i is $\pm 1/2$ while the total S_z of all sites is zero. We define the following time correlator for σ_z as

$$I(t) = \frac{4}{L} \sum_{j=1}^{L} \langle \Psi(0) | S_j^z(0) S_j^z(t) | \Psi(0) \rangle \,, \tag{2.2}$$

which detects the total imbalance of spin-z component. As shown in Fig. 2.5(a), we find a systematic change of the properties of $I(t)$ as W is varied. For smaller $W = 0.5$ and 1, we see that the long time behavior of imbalance $I(t)$ is dominated by power-law decay $t^{-\zeta}$, and at the large t limit S_i^z on a site becomes uncorrelated with the initial condition and $I(t)$ approaches zero. For intermediate $W = 1.5$ and 2, a similar power-law behavior is obtained with a much smaller decay power ζ, indicating the longer time scale required to approach equilibrium spin correlations for these thermal states near the transition point to the MBL

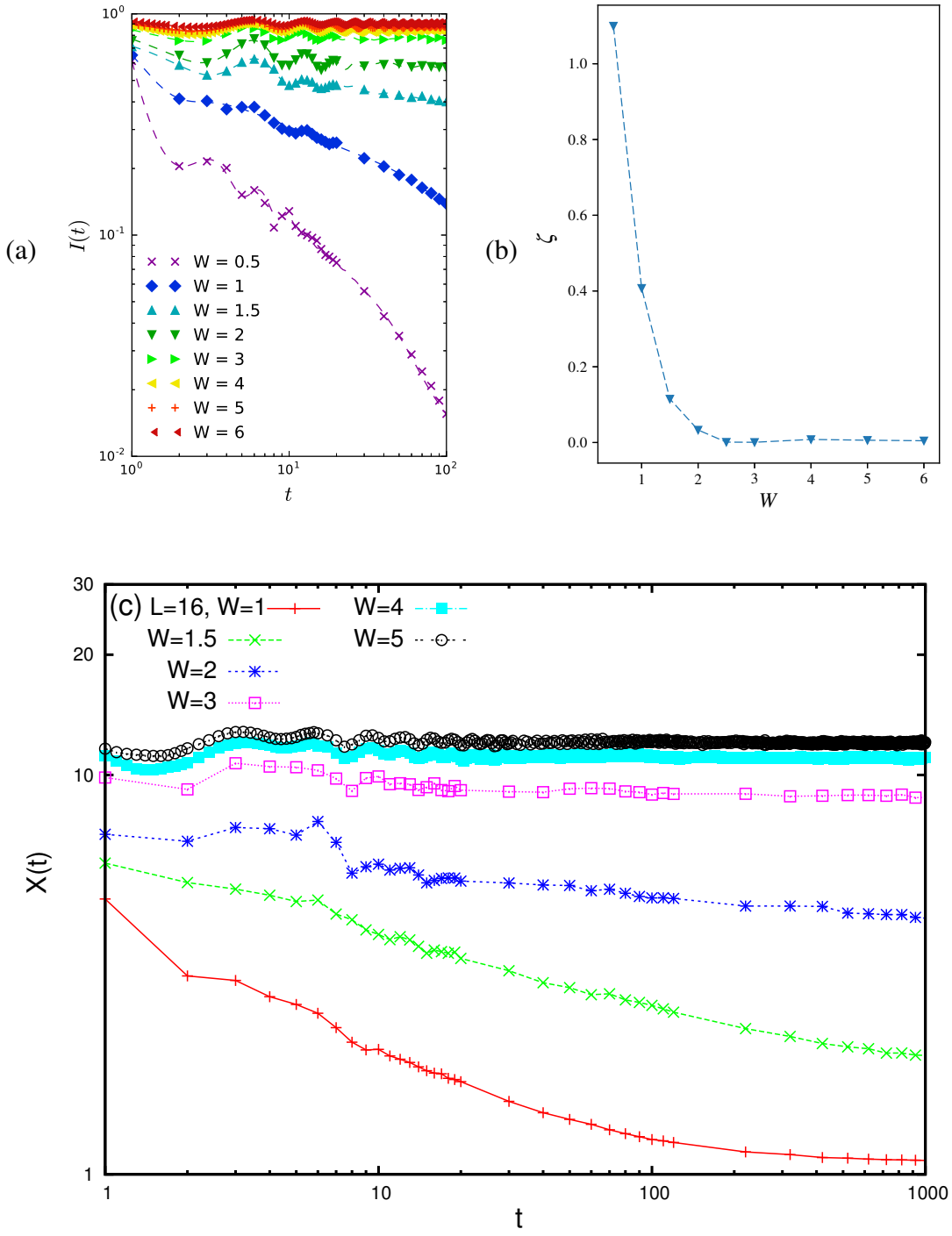

Figure 2.5: (a) Imbalance $I(t)$ for a $L = 16$ system with $W = 0.5 - 6$. At small values of W, we notice the $I(t)$ of the system decays rapidly; however, when W is increased beyond $W > 2$, $I(t)$ ceases decaying and remains at a certain level. This is consistent with the MBL behavior where the initial values of the local observables for each site i is preserved. (b) Fitting parameter ζ for the power-law decay exponent as a function of W. (c) Spin glass order as defined in eq.2.3. At small values of W, correlations between spins are short ranged and $\chi(t)$ decays to 1 over time; at large values of W, $\chi(t)$ remains close to its initial value even at very long time, further corroborating our assertion of a quantum phase transition.

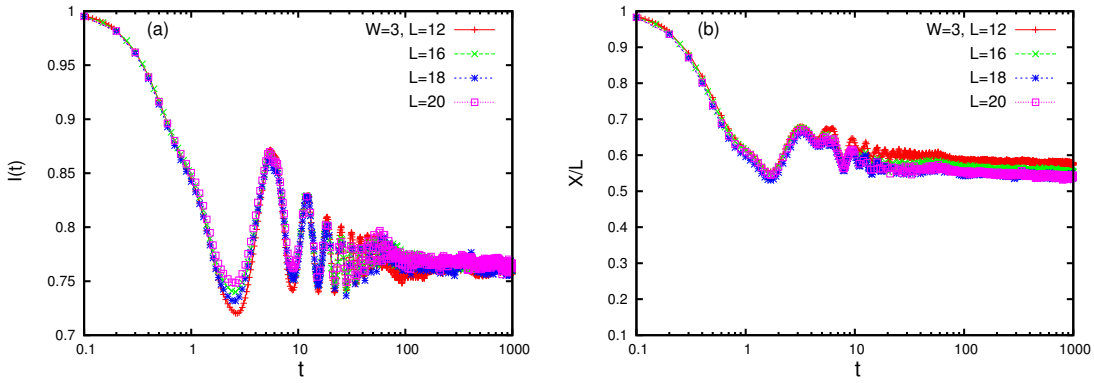

Figure 2.6: (a) Imbalance $I(t)$ for a $L = 12 - 20$ systems at $W = 3$. $I(t)$ is insensitive to system size L. It shows initial oscillation at shorter times, and it stays at nonzero value at the long time limit. (b) Spin glass order $\chi(t)/L$ saturates to finite nonzero value indicating the divergent behavior with L.

phase. On the MBL side with $W = 3$ and 4, we see that the $I(t)$ is near constant at large t limit with a near vanishing decay exponent ($\zeta \sim 0$). In Fig. 2.5(b), we show the decay exponent ζ as a function of W, where we find that the critical point for the transition to MBL phase is close to $W_c \sim 2.5$ consistent with the conjecture that $W_c \sim 1.85$ is only the lower bound of the critical point, though for given range of system sizes $L = 10 - 18$ it does give the best collapsing of the finite sizes entropy and fluctuation data (for highly excited eigenstates) as shown in Fig. 2.2.

For comparison, we also study spin glass order [29] for the MBL phase. The spin-flip from the Heisenberg term will create domain walls. If the domain walls are confined together, a spin-glass order can develop. We define the spin glass order parameter

$$\chi = \frac{1}{L} \sum_{i,j=1}^{L} \langle \Psi(t)|4S_i^z S_j^z|\Psi(t)\rangle^2 , \tag{2.3}$$

which can diverge with L in the spin-glass ordered phase. As shown in Fig. 2.5(c), we see behavior very similar to $I(t)$. For smaller $W = 1 - 2$, we see that $\chi(t)$ decreases with t in power-law fashion, while it maintains a large value in the long time limit for larger $W > 2$. Our results indicate a jump of the spin glass order at the thermal to MBL transition. In Fig. 2.6, we see that both $I(t)$ and $\chi(t)/L$ show very weak size dependence at $W = 3$ and remain

nonzero at long time and large system size limits, which fully establish the robustness of the MBL phase.

2.3 Summary and Discussions

We have studied many-body localization and quantum phase transitions in spin chain systems in the presence of quasiperiodic fields. Based on the entanglement entropy and the fluctuation of the half system magnetization studies, we find the lower bound of the critical field strength W_c for the dynamic quantum phase transition from the thermal phase to the MBL phase driven by the quasiperiodic fields to be on the order of $W_c \sim 1.85$. Interestingly, for W just above W_c, we find that the entanglement entropy following a global quench grows with time under the power law, consistent with the behavior of the thermal phase. From the scaling behavior of the spin imbalance and spin glass order, we identify the divergent spin glass order for $W \geq 3$. Overall, the finite size effect in such a quasiperiodic system turns out to be not too important as the scaling behavior in the intermediate regime near the transition appears to be showing either thermal behavior ($W \sim 2$) or MBL characteristics ($W \sim 3$), suggesting the best estimate of the transition point to be $W_c \sim 2.5$. Our results provide quantitative understanding of the effect of quasiperiodic fields, which are more efficient in driving MBL physics than random fields due to importance of the rare Griffiths regions in random field models. Our results are also consistent with experimentally observed MBL phenomena [61] for one dimensional fermionic systems with quasiperiodic fields through a Jordan-Wigner transformation. In such experimental systems, while the fermionic interaction term enhances delocalization similar to the effect of spin-spin interaction, MBL is stabilized by the quasi-field. In Chapter 3, we will examine the mobility edge [67] in such systems by probing different energy densities and using density matrix renormalization group methods.

Chapter 3

Mobility edge in spin chain systems with quasiperiodic fields

The work of Ref. [2] predicted an MBL transition occurring at finite temperature with a many-body mobility edge (MBME) and ED studies have reported the appearance of MBMEs in small 1D and ladder systems [23, 29, 51, 73]. However, studies with other methods on larger systems did not find similar evidence [79, 80] and numerical linked cluster expansion suggests the extent of the localized phase could be overstated [24]. Furthermore, theoretical arguments have been put forth suggesting scenarios where fluctuations into the ergodic phase from the local phase could induce global delocalization [81]. Such a scenario would prevent an MBME from existing, and the authors suggest that finite-size effects cannot be ruled out for the appearance of MBMEs in previously studied systems [81].

In this chapter, we study spin chain systems with quasiperiodic fields at various energy densities in order to see if there is a qualitative difference in the appearance of an MBME between quasiperiodic fields and previously studied random field models. We test the use of Density Matrix Renormalization Groups (DMRG) for evaluating finite-size effects in the appearance of MBMEs.

3.1 Crossing of entanglement entropy

Using the ED calculations outlined in Chapter 2, and the same model, we study the behavior of scaled entanglement entropy S/L verses disorder W at different energy densities ϵ between $\epsilon = 0.2$ to $\epsilon = 0.5$. We choose to focus on the low energy density behavior as we can extrapolate qualitative features into regimes accessible by DMRG. For smaller ϵ, care must be taken to ensure that the average energy of the kept eigenpairs corresponds to the target energy E defined by $\epsilon = (E - E_0)/(E_{max} - E_0)$. For example, at $L = 10$ and $\epsilon = 0.1$, the target energy typically lies between the ground state and first excited state, thus only two

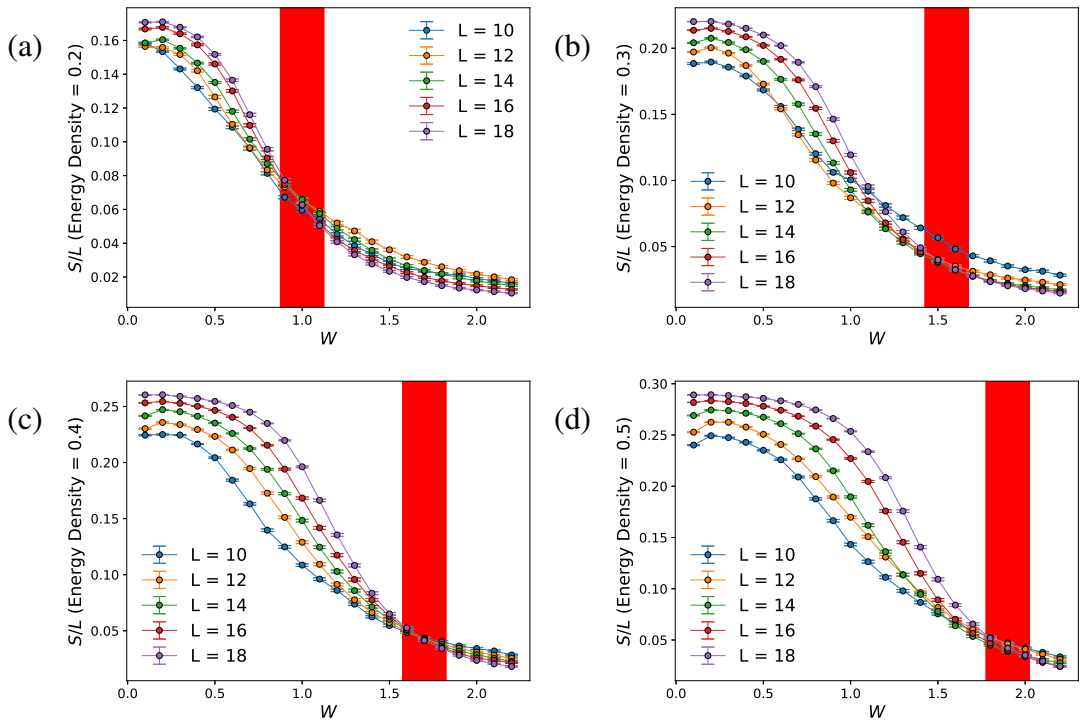

Figure 3.1: Observed shift in crossing point for S/L vs W curves as energy density ϵ is varied, consistent with a finite size mobility edge.

eigenpairs can be kept. While this makes $L = 10$ calculations less reliable near the ends of the energy spectrum, larger system sizes are less susceptible to this issue.

In Figure 3.1, we observe crossings at $W \sim 1.00$ for $\epsilon = 0.2$, $W \sim 1.55$ for $\epsilon = 0.3$, $W \sim 1.65$ for $\epsilon = 0.4$, and $W \sim 1.85$ for $\epsilon = 0.5$. This observed shift in the critical disorder strength W_c with respect to energy density ϵ appears to be a mobility edge, although we have not ruled out finite-size effects.

3.2 Probability distributions of entanglement entropy

Another method of studying the MBL transition is to examine the probability distributions of the entanglement entropy [49, 51, 59, 82]. Previous studies have found that entanglement entropy appears normally distributed at low disorder, begin to develop exponential tails at intermediate disorder, and transition to long-tailed distributions with characteristic peaks at

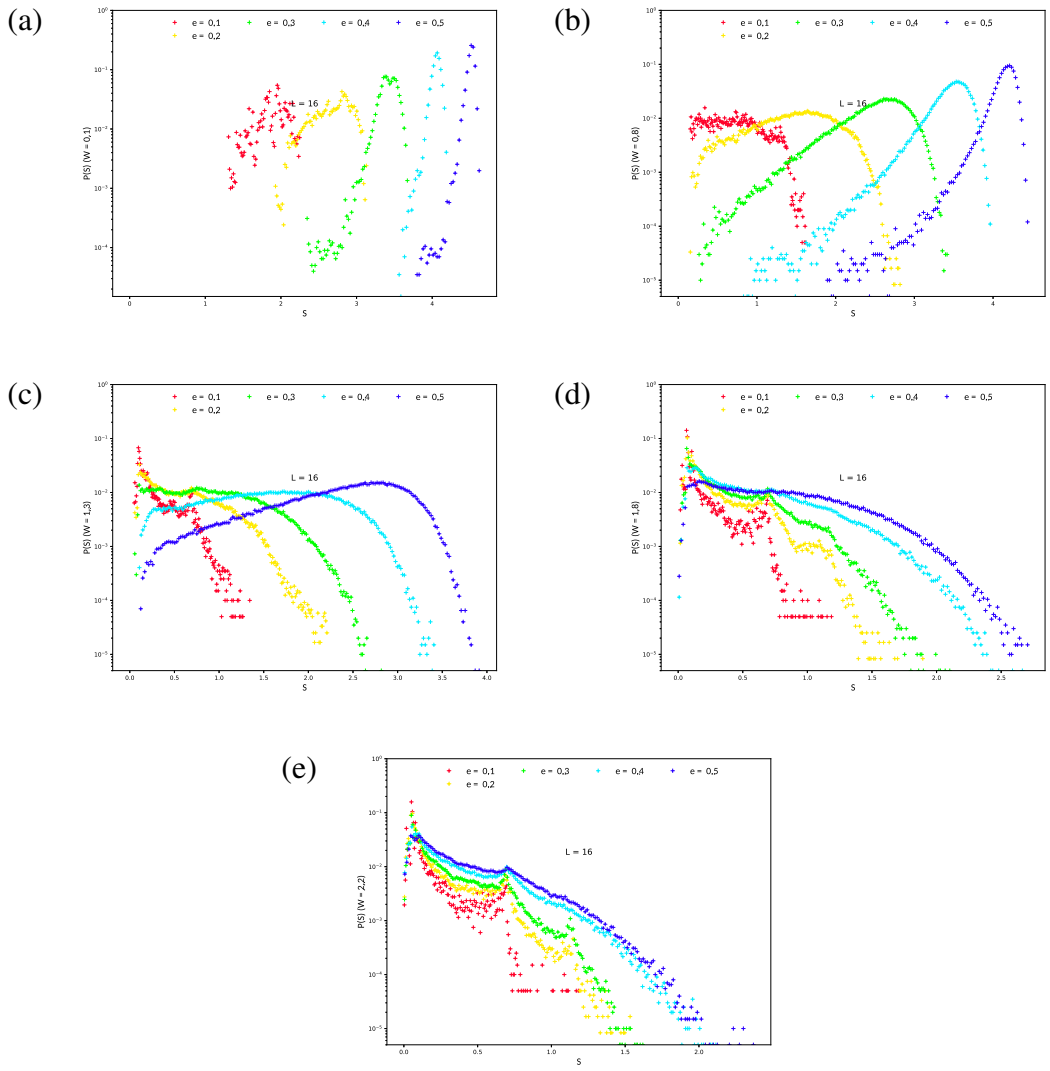

Figure 3.2: Observed transitions from normal to long-tailed distributions as W is increased. Transitions appear to occur at lower disorder for smaller energy density.

$S = 0$ and $S = \ln 2$. This behavior can be used to characterize the ergodic and MBL phases by their probability distributions. We study the probability distributions of entanglement entropy S at fixed system size $L = 16$ at different energy densities ϵ and disorder strengths W. At low disorder strength $W = 0.1$, entanglement entropy appears to be normally distributed across all energy densities as would be expected in the thermal phase. As we increase disorder, we begin to see transitions into the long-tailed distributions that are characteristic of the MBL phase. These transitions begin to occur earlier for lower energy density providing more qualitative evidence of an MBME in small systems. We also see an additional peak form at $S = \ln 3$.

3.3 Density matrix renormalization group

The size of systems accessible to ED calculations is severely limited because the Hilbert space grows exponentially with system size as 2^L. However, in certain systems, the relevant physics may be contained in a small subspace. Density Matrix Renormalization Group (DMRG) [83] methods exploit this property to calculate the ground state of large and even infinite sized systems MBL states also have a reduced state space bound by the area law and there have been recent efforts to exploit this in order to target highly excited states of MBL systems [57, 59].

Consider a system consisting of a left block A and a right block B which contain one spin each at the start. Insert a pair of spins in between the blocks creating a *superblock* A••B. This structure can then be separated again into a new A and B blocks consisting of the previous block-site A• and site-block •B, respectively. The Hilbert space of the superblock is still exponential 2^l, the crucial step is to reduce the state space through a process called *decimation*: (1) Diagonalize the superblock Hamiltonian $\hat{H}_{A\bullet\bullet B}$ using a sparse eigensolver to obtain the groundstate. (2) Find the reduced density matrix $\rho_{A\bullet}$ for the left block-site subsystem. (3) Diagonalize $\rho_{A\bullet}$ to obtain the largest m eigenpairs, w_a and

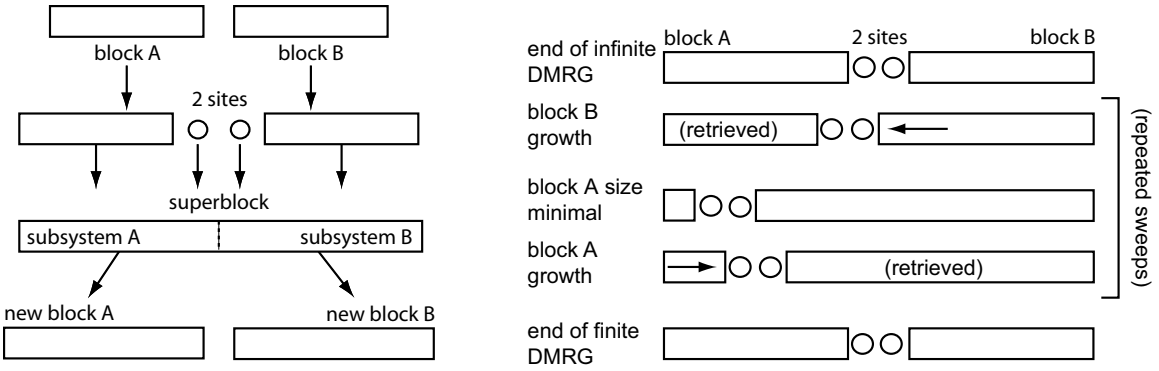

Figure 3.3: The left and right half of the figure present the iterations taken in the infinite-system and finite-system DMRG procedures respectively. In both cases, new blocks are formed from integrating a site into a block, with a state space truncation according to the density-matrix prescription of DMRG. Whereas in the infinite-system version this growth happens on both sides of the chain, leading to chain growth, in the finite-system algorithm it happens only for one side at the expense of the other, leading to constant chain length. From Ref. [84]

$|u^a\rangle$ with $a = 1, \ldots, m$ and $m < l$. (4) Construct an operator $\hat{O}$ of dimension $m \times l$ whose rows are $|u^a\rangle$ and create a reduced Hamiltonian $\hat{H}_{A'} = \hat{O}\hat{H}_{A\bullet\bullet B}\hat{O}^\dagger$. (5) Replace block A with A', and by similar procedure replace B with B'.

This process of iteratively growing the system is known as infinite-system DMRG. Once the system is grown to the desired size finite-sized DMRG can be used to improve the approximation of ground state. This process grows block A(B) at the expense of block B(A), utilizing previously obtained smaller block B(A) operators. This process is swept back and forth repeatedly until convergence on the desired state is achieved. The error associated with truncating states in this manner is given by $\epsilon_T = 1 - \sum_1^m w_a$.

In order to target excited states, we used a modified version of DMRG called En-DMRG [59]. The standard DMRG algorithm is modified at the finite-system stage. Here we use the six lowest eigenstates of the squared Hamiltonian $\hat{H}_2 = (\hat{H} - E_t\hat{I})^2$ where E_t is the target energy and $\hat{I}$ is an identity matrix of appropriate dimension. We use the En-DMRG method to target energies at our desired energy density $\epsilon = (E_t - E_{min})/(E_{max} - E_{min})$. We conduct our En-DMRG calculations at $\epsilon = 0.1$ and $W = 1.8$ which, according to our ED calculations, should be deep in the MBL phase. As seen in Fig. 3.4, we observe that scaled

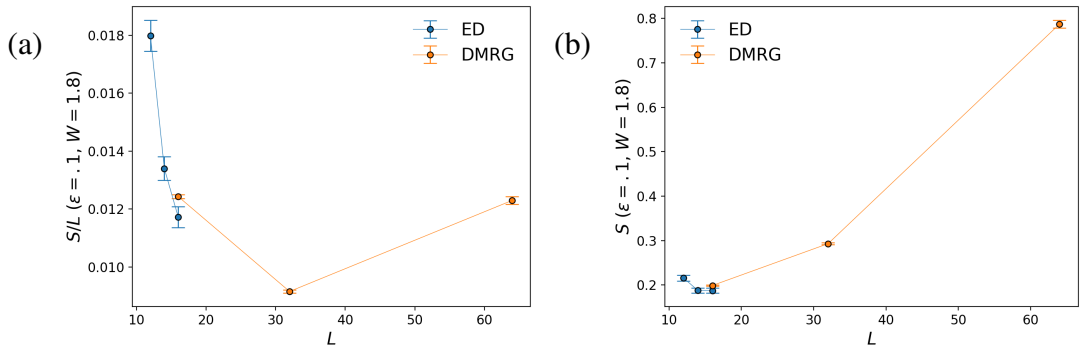

Figure 3.4: (a) Scaled and (b) unscaled entanglement entropy versus system size. We observe different scaling behavior for our largest system size $L = 64$ suggesting more study might elucidate the nature of finite size effects on the appearance of a mobility edge.

entropy S/L decreases with increased system size L in both ED and En-DMRG calculations up to size $L = 32$. However, we see an increase at $L = 64$, indicating possible thermal scaling. While these initial observations are far from conclusive, they are a potentially exciting glimpse into finite-size effects on the appearance of the mobility edge.

3.4 Summary and discussion

Utilizing established ED methods, we demonstrate the appearance of a mobility edge in small spin-chain systems with quasiperiodic fields up to size $L = 18$. However, finite size effects cannot be ruled out. Utilizing the recently developed En-DMRG [59] method, our exploratory calculation gives an anomalous data point at size $L = 64$ where scaling of entropy S/L is inconsistent with a localized phase. While improvements to the reliability and efficiency of the En-DMRG method must be made, it appears that there are insights to be gained by studying system sizes accessible to this method. Another interesting direction is to explore the MBL phase transition in ladder systems with coupled spin chains [51], which provides information about the MBL physics in two dimensions.

Bibliography

[1] P. W. Anderson, Phys. Rev. **109**, 1492 (1958).

[2] D. M. Basko, I. L. Aleiner, and B. L. Altshuler, Annals of Physics **321**, 1126 (2006).

[3] V. Oganesyan and D. A. Huse, Phys. Rev. B **75**, 155111 (2007).

[4] A. Pal and D. A. Huse, Phys. Rev. B **82**, 174411 (2010).

[5] M. Žnidarič, T. Prosen, and P. Prelovšek, Phys. Rev. B **77**, 064426 (2008).

[6] D. A. Huse, R. Nandkishore, V. Oganesyan, A. Pal, and S. L. Sondhi, Phys. Rev. B **88**, 014206 (2013).

[7] R. Nandkishore and D. A. Huse, Annu. Rev. Condens. Matter Phys. **6**, 15 (2015).

[8] E. Altman and R. Vosk, Annu. Rev. Condens. Matter Phys. **6**, 383 (2015).

[9] D. A. Huse, R. Nandkishore, and V. Oganesyan, Phys. Rev. B **90**, 174202 (2014).

[10] R. Nandkishore, S. Gopalakrishnan, and D. A. Huse, Phys. Rev. B **90**, 064203 (2014).

[11] D. Pekker, G. Refael, E. Altman, E. Demler, and V. Oganesyan, Phys. Rev. X **4**, 011052 (2014).

[12] M. Rigol, V. Dunjko, and M. Olshanii, Nature **452**, 854 (2008).

[13] M. Serbyn et al., Phys. Rev. Lett. **113**, 147204 (2014).

[14] M. P. Kwasigroch and N. R. Cooper, Phys. Rev. A **90**, 021605 (2014).

[15] N. Yao et al., Phys. Rev. Lett. **113**, 243002 (2014).

[16] R. Vasseur, S. A. Parameswaran, and J. E. Moore, Phys. Rev. B **91**, 140202 (2015).

[17] M. Serbyn, Z. Papić, and D. A. Abanin, Phys. Rev. Lett. **111**, 127201 (2013).

[18] V. Ros, M. Müller, and A. Scardicchio, Nuclear Physics B **891**, 420 (2015).

[19] A. Chandran, V. Khemani, C. R. Laumann, and S. L. Sondhi, Phys. Rev. B **89**, 144201 (2014).

[20] T. Grover, arXiv:1405.1471 [cond-mat, physics:quant-ph] (2014), arXiv: 1405.1471.

[21] K. Agarwal, S. Gopalakrishnan, M. Knap, M. Müller, and E. Demler, Phys. Rev. Lett. **114**, 160401 (2015).

[22] S. Gopalakrishnan et al., Phys. Rev. B **92**, 104202 (2015).

[23] D. J. Luitz, N. Laflorencie, and F. Alet, Phys. Rev. B **91**, 081103 (2015).

[24] T. Devakul and R. R. Singh, Phys. Rev. Lett. **115**, 187201 (2015).

[25] E. J. Torres-Herrera and L. F. Santos, Phys. Rev. B **92**, 014208 (2015).

[26] E. Canovi, D. Rossini, R. Fazio, G. E. Santoro, and A. Silva, Phys. Rev. B **83**, 094431 (2011).

[27] E. Cuevas, M. Feigel'man, L. Ioffe, and M. Mezard, Nature Communications **3**, 1128 (2012).

[28] B. Bauer and C. Nayak, J. Stat. Mech. **2013**, P09005 (2013).

[29] J. A. Kjäll, J. H. Bardarson, and F. Pollmann, Phys. Rev. Lett. **113**, 107204 (2014).

[30] A. D. Luca and A. Scardicchio, EPL **101**, 37003 (2013).

[31] S. Iyer, V. Oganesyan, G. Refael, and D. A. Huse, Phys. Rev. B **87**, 134202 (2013).

[32] S. Johri, R. Nandkishore, and R. Bhatt, Phys. Rev. Lett. **114**, 117401 (2015).

[33] J. H. Bardarson, F. Pollmann, and J. E. Moore, Phys. Rev. Lett. **109**, 017202 (2012).

[34] F. Andraschko, T. Enss, and J. Sirker, Phys. Rev. Lett. **113**, 217201 (2014).

[35] C. Laumann, A. Pal, and A. Scardicchio, Phys. Rev. Lett. **113**, 200405 (2014).

[36] J. M. Hickey, S. Genway, and J. P. Garrahan, J. Stat. Mech. **2016**, 054047 (2016).

[37] A. Nanduri, H. Kim, and D. A. Huse, Phys. Rev. B **90**, 064201 (2014).

[38] Y. Bar Lev and D. R. Reichman, Phys. Rev. B **89**, 220201 (2014).

[39] J. Z. Imbrie, J Stat Phys **163**, 998 (2016).

[40] T. Grover and M. P. A. Fisher, J. Stat. Mech. **2014**, P10010 (2014).

[41] P. Ponte, Z. Papić, F. Huveneers, and D. A. Abanin, Phys. Rev. Lett. **114**, 140401 (2015).

[42] Y. Huang, arXiv:1507.01304 [cond-mat] (2015), arXiv: 1507.01304.

[43] Y.-Z. You, X.-L. Qi, and C. Xu, Phys. Rev. B **93**, 104205 (2016).

[44] M. Serbyn and J. E. Moore, Phys. Rev. B **93**, 041424 (2016).

[45] R. Singh, J. H. Bardarson, and F. Pollmann, New J. Phys. **18**, 023046 (2016).

[46] Y. B. Lev and D. R. Reichman, EPL **113**, 46001 (2016).

[47] D.-L. Deng, J. H. Pixley, X. Li, and S. Das Sarma, Phys. Rev. B **92**, 220201 (2015).

[48] X. Chen, X. Yu, G. Y. Cho, B. K. Clark, and E. Fradkin, Phys. Rev. B **92**, 214204 (2015).

[49] R. Vosk, D. A. Huse, and E. Altman, Phys. Rev. X **5**, 031032 (2015).

[50] A. C. Potter, R. Vasseur, and S. Parameswaran, Phys. Rev. X **5**, 031033 (2015).

[51] E. Baygan, S. P. Lim, and D. N. Sheng, Phys. Rev. B **92**, 195153 (2015).

[52] L. Zhang, B. Zhao, T. Devakul, and D. A. Huse, Phys. Rev. B **93**, 224201 (2016).

[53] L. Zhang, V. Khemani, and D. A. Huse, Phys. Rev. B **94**, 224202 (2016).

[54] X. Yu, D. J. Luitz, and B. K. Clark, Phys. Rev. B **94**, 184202 (2016).

[55] V. Khemani, D. Sheng, and D. A. Huse, Phys. Rev. Lett. **119**, 075702 (2017).

[56] P. T. Dumitrescu, R. Vasseur, and A. C. Potter, Physical Review Letters **119** (2017), arXiv: 1701.04827.

[57] V. Khemani, F. Pollmann, and S. Sondhi, Phys. Rev. Lett. **116**, 247204 (2016).

[58] X. Yu, D. Pekker, and B. K. Clark, Phys. Rev. Lett. **118**, 017201 (2017).

[59] S. P. Lim and D. N. Sheng, Phys. Rev. B **94**, 045111 (2016).

[60] D. M. Kennes and C. Karrasch, Phys. Rev. B **93**, 245129 (2016).

[61] M. Schreiber et al., Science **349**, 842 (2015).

[62] P. Bordia et al., Phys. Rev. Lett. **116**, 140401 (2016).

[63] H. P. Lüschen et al., arXiv:1612.07173 [cond-mat, physics:quant-ph] (2016), arXiv: 1612.07173.

[64] H. P. Lüschen et al., Phys. Rev. X **7**, 011034 (2017).

[65] S. Nag and A. Garg, Physical Review B **96** (2017), arXiv: 1701.00236.

[66] Y. B. Lev, D. M. Kennes, C. Klöckner, D. R. Reichman, and C. Karrasch, EPL (Europhysics Letters) **119**, 37003 (2017), arXiv: 1702.04349.

[67] T. Roscilde, P. Naldesi, and E. Ercolessi, SciPost Physics **1**, 010 (2016).

[68] R. Modak and S. Mukerjee, Phys. Rev. Lett. **115**, 230401 (2015).

[69] D.-L. Deng et al., ANNALEN DER PHYSIK **529**, n/a (2017).

[70] D. J. Luitz, N. Laflorencie, and F. Alet, Phys. Rev. B **93**, 060201 (2016).

[71] A. C. Potter and A. Vishwanath, arXiv:1506.00592 [cond-mat] (2015), arXiv: 1506.00592.

[72] H. F. Song et al., Phys. Rev. B **85**, 035409 (2012).

[73] I. Mondragon-Shem, A. Pal, T. L. Hughes, and C. R. Laumann, Physical Review B **92** (2015), arXiv: 1501.03824.

[74] A. Einstein, B. Podolsky, and N. Rosen, Physical Review **47**, 777 (1935).

[75] V. Khemani, S. Lim, D. Sheng, and D. A. Huse, Phys. Rev. X **7**, 021013 (2017).

[76] S. Aubry and G. André, Ann. Israel Phys. Soc **3**, 18 (1980).

[77] P. Bordia, H. Lüschen, U. Schneider, M. Knap, and I. Bloch, Nature Physics **13**, 460 (2017).

[78] D. N. Page, Phys. Rev. Lett. **71**, 1291 (1993).

[79] G. Carleo, G. Boéris, M. Holzmann, and L. Sanchez-Palencia, Physical Review Letters **111**, 050406 (2013).

[80] B. Tang, D. Iyer, and M. Rigol, Physical Review B **91**, 161109 (2015).

[81] W. de Roeck, F. Huveneers, M. Müller, and M. Schiulaz, Physical Review B **93** (2016), arXiv: 1506.01505.

[82] D. J. Luitz, Physical Review B **93**, 134201 (2016).

[83] S. R. White, Physical Review Letters **69**, 2863 (1992).

[84] U. Schollwöck, Annals of Physics **326**, 96 (2011).

[85] M. Lee, T. R. Look, S. P. Lim, and D. N. Sheng, Phys. Rev. B **96**, 075146 (2017).

Appendix A

Works associated with this thesis

En route to the completion of this thesis, our findings which comprise Chapter 2 were published in Physical Review B [85]. It appears in this work in a slightly modified form, although the copyright to the original publication remains with the journal. I made significant contributions to this work as co-lead author.

The following public presentations were based on materials from this thesis:

1. *Many-Body Localization and Mobility Edge in Spin-Chain Systems With Quasiperiodic Fields*
   (a) Talk at CSUNposium, April 2018
   (b) Talk at APS March Meeting, March 2018
2. *Many-Body Localization in Spin-Chain Systems With Quasiperiodic Fields*
   (a) Talk at CSUNposium, April 2017